

# Effects of thin metal contacts on few-layer van der Waals ferrielectric $\text{CuInP}_2\text{S}_6$


Cite as: J. Appl. Phys. **132**, 114102 (2022); <https://doi.org/10.1063/5.0096704>

Submitted: 20 April 2022 • Accepted: 12 August 2022 • Published Online: 16 September 2022

 Andrew O'Hara, Lei Tao,  Sabine M. Neumayer, et al.

## COLLECTIONS

Paper published as part of the special topic on [2D Piezoelectrics, Pyroelectrics, and Ferroelectrics](#)

 This paper was selected as Featured



View Online



Export Citation



CrossMark

## ARTICLES YOU MAY BE INTERESTED IN

[Influence of structural properties on the ferroelectric behavior of hexagonal  \$\text{AlScN}\$](#)

Journal of Applied Physics **132**, 114101 (2022); <https://doi.org/10.1063/5.0103578>

[Correlative piezoresponse and micro-Raman imaging of  \$\text{CuInP}\_2\text{S}\_6\$ - \$\text{In}\_{4/3}\text{P}\_2\text{S}\_6\$  flakes unravels phase-specific phononic fingerprint via unsupervised learning](#)

Applied Physics Letters **121**, 062901 (2022); <https://doi.org/10.1063/5.0101395>

[Tin removal by an annular surface wave plasma antenna in an extreme ultraviolet lithography source](#)

Journal of Applied Physics **132**, 113302 (2022); <https://doi.org/10.1063/5.0094375>

Webinar

Meet the Lock-in Amplifiers  
that measure microwaves

Oct. 6th – Register now



Zurich  
Instruments



# Effects of thin metal contacts on few-layer van der Waals ferrielectric $\text{CuInP}_2\text{S}_6$

Cite as: J. Appl. Phys. **132**, 114102 (2022); doi: [10.1063/5.0096704](https://doi.org/10.1063/5.0096704)

Submitted: 20 April 2022 · Accepted: 12 August 2022 ·

Published Online: 16 September 2022



Andrew O'Hara,<sup>1</sup> Lei Tao,<sup>1,2</sup> Sabine M. Neumayer,<sup>3</sup> Petro Maksymovych,<sup>3</sup> Nina Balke,<sup>3,4</sup> and Sokrates T. Pantelides<sup>1,5,a)</sup>

## AFFILIATIONS

<sup>1</sup>Department of Physics and Astronomy, Vanderbilt University, Nashville, Tennessee 37235, USA

<sup>2</sup>Institute of Physics, Chinese Academy of Sciences, University of Chinese Academy of Sciences, Beijing 100190, China

<sup>3</sup>Center for Nanophase Materials Sciences, Oak Ridge National Laboratory, Oak Ridge, Tennessee 37831, USA

<sup>4</sup>Department of Materials Science and Engineering, North Carolina State University, Raleigh, North Carolina 27695, USA

<sup>5</sup>Department of Electrical and Computer Engineering, Vanderbilt University, Nashville, Tennessee 37235, USA

**Note:** This paper is part of the Special Topic on 2D Piezoelectrics, Pyroelectrics, and Ferroelectrics.

**a) Author to whom correspondence should be addressed:** [pantelides@vanderbilt.edu](mailto:pantelides@vanderbilt.edu)

## ABSTRACT

Out-of-plane polarized ferroelectric materials in a capacitive structure provide a key component for several technological applications. Furthermore, two-dimensional materials are expected to aid in the quest for both ultrathin and flexible electronics. Of the various two-dimensional ferroelectrics with out-of-plane polarization,  $\text{CuInP}_2\text{S}_6$  is special in that the Cu atoms are highly mobile and it has been shown to possess both low- and high-polarization states. Using density-functional-theory calculations, we explore the stabilization of the ferroelectric state for several prototypical metal contacts (Gr, Ni, Cu, Au, and Ag). In all cases, we find that the ferroelectric state can be stabilized at fewer layers than in the freestanding case. For all of the considered conventional metal contacts, we also find the existence of a quasi-ferroelectric state that stabilizes a polar phase for thicknesses greater than two layers of CIPS. In the cases of Au and Ag, interfacial alignment and strain can be used to stabilize ferroelectricity at the bilayer limit. Furthermore, we find that the strength of the interaction between the contact and  $\text{CuInP}_2\text{S}_6$  also leads to stabilization of the high-polarization state when ferroelectricity is stabilized. Lastly, energy-barrier calculations show that the system is still switchable in the presence of contact doping from the metal contacts.

Published under an exclusive license by AIP Publishing. <https://doi.org/10.1063/5.0096704>

## I. INTRODUCTION

The ferroelectric capacitor, which consists of a ferroelectric material sandwiched between two conducting materials, is a key component for various electronic device applications including ferroelectric tunnel junctions,<sup>1–3</sup> nonvolatile memories,<sup>4</sup> and energy storage.<sup>4,5</sup> However, when the thickness of a ferroelectric reaches the order of tens or fewer nanometers, size effects impose fundamental limits on their performance. Via phenomenological electrostatic arguments, the primary limiting factor for ultrathin ferroelectrics is believed to be the long-range depolarization field arising from surface or interfacial dipoles, which competes with the intrinsic coercive fields of the ferroelectric.<sup>6–9</sup> Surface or interface dipoles are generated by several mechanisms, including electrostatic barrier formation,<sup>6</sup> point defects,<sup>6,9,10</sup> ionic screening,<sup>11–13</sup> and

surface damage<sup>6,9</sup> to name a few. In the widely studied ferroelectric perovskite-structure oxides, the Curie temperature decreases as the thickness decreases,<sup>14</sup> and the polarization is suppressed<sup>15</sup> or even disappears<sup>16</sup> when the thickness reaches a critical value. Beyond the suppression of the Curie temperature and spontaneous polarization, depolarizing fields may influence the domain structure<sup>17,18</sup> and create ferroelectric dead layers.<sup>19,20</sup>

The properties of the metal–ferroelectric interface are considered to be one of the most important factors in controlling ferroelectric behavior.<sup>8,21</sup> Although the ferroelectric-metal interface often creates a strong depolarization field due to incomplete surface screening, it may also effectively strengthen the screening of bound charges at the interface.<sup>16,22</sup> Furthermore, studies have shown that while perovskite ferroelectrics such as  $\text{BaTiO}_3$  and  $\text{PbTiO}_3$  often

have a critical thickness of several nanometers, the use of strain<sup>23</sup> or structurally compatible oxide-based contacts<sup>7,24</sup> can maintain ferroelectricity down to  $\sim 1$  nm.

Layered, van-der-Waals-bonded, two-dimensional (2D) ferroelectric materials possessing out-of-plane polarization, such as  $\text{CuInP}_2\text{S}_6$  (CIPS),<sup>25</sup>  $\alpha\text{-In}_2\text{Se}_3$ ,<sup>26</sup> and  $\text{d1T-MoTe}_2$ ,<sup>27</sup> are promising candidates for ultrathin ferroelectric capacitive nano-devices. Each of these materials has unusual properties. It was predicted by theory and confirmed by experiments that CIPS features a strain-tunable quadruple-well energy profile,<sup>28</sup> which accounts for the existence of two low-polarization (LP) and two high-polarization (HP) states,<sup>29,30</sup> and leads to multiple polarization loops.<sup>28</sup> The HP states are enabled by Cu atoms moving just past the layer edges and bonding to sulfur atoms in the adjacent layers across the van der Waals (vdW) gaps.<sup>28,30</sup> In addition, an electric field can push the Cu atoms across the van-der-Waals gap, giving rise to a polarization that is directed against the electric field and novel polarization loops.<sup>31,32</sup> Furthermore, the high mobility of Cu atoms can lead to unique switching pathways through the layers for domain inversion.<sup>33</sup>  $\alpha\text{-In}_2\text{Se}_3$  exhibits a large tunability of its bandgap due to strong quantum confinement effects,<sup>34</sup> a Curie temperature well above room temperature even at the ultrathin limit,<sup>35</sup> and the unusual property of “polarization locking” in which an in-plane electric field can be used to switch the larger out-of-plane component of polarization.<sup>36</sup> Finally,  $\text{MoTe}_2$  and select other dichalcogenides with the  $\text{MoS}_2$  structure feature an unusual form of improper ferroelectricity,<sup>37,38</sup> electric-field-induced strain conversion of a semimetallic to a ferroelectric semiconducting phase,<sup>39</sup> and even novel topological phases.<sup>40</sup>

In general, the absence of dangling bonds on the surfaces of 2D materials and the weaker van der Waals (vdW) bonding provides a means of reducing the number of interface defects,<sup>41</sup> which in turn may reduce the effects of one source of depolarizing fields. Theoretical calculations show that for the quintuple-layer  $\alpha\text{-In}_2\text{Se}_3$ , depolarizing effects are relatively minor with robust ferroelectricity in the freestanding structure and only a small reduction for graphene electrodes.<sup>26</sup> On the other hand, for trimerized  $\text{d1T-MoTe}_2$ , the freestanding material's polarization originating from the asymmetry generated by the Mo-trimer formation is offset by an inward dimpling of the Te atoms.<sup>27</sup> For CIPS, the effect of the depolarization field results in an antiferroelectric ground state in both monolayer<sup>42</sup> and few-layer<sup>43</sup> freestanding CIPS and other similar materials. Owing to the order-disorder nature of the local dipoles in CIPS,<sup>29,44</sup> the monolayer structure has an intralayer antiferroelectric state with alternating in-plane dipole directions<sup>42,45</sup> that can be reverted back to a ferroelectric ground state under strain.<sup>42</sup> For few-layer structures of two through four layers, CIPS adopts an interlayer AFE state in which individual layers are coupled ferroelectrically and alternate from layer-to-layer with copper preferring the internal sides of the surface layers.<sup>43</sup>

The aforementioned 2D ferroelectrics provide opportunities to fabricate tunable electronics based on vdW heterostructures, such as ferroelectric field effect transistors (Fe-FET),<sup>46</sup> negative-capacitance field effect transistors (NC-FET),<sup>47</sup> ferroelectric junctions,<sup>48,49</sup> and nonvolatile memories.<sup>50,51</sup> Despite the promise of these vdW layered, out-of-plane polarized ferroelectrics, presently there are no comprehensive studies on the metal/2D-ferroelectric

interface focusing on thickness or contact-type dependence at the ultrathin limit. Quantitative understanding of the effects of metal contacts on the properties of ultrathin vdW and 2D ferroelectrics is a timely topic that can impact the further development and engineering of nanodevices based on these materials.

In this paper, we use density-functional-theory (DFT) calculations to investigate the effect of metal contacts on 2D ferroelectrics with out-of-plane polarization, focusing primarily on  $\text{CuInP}_2\text{S}_6$ . For the contact interfaces to CIPS, we consider four prototypical metals, namely, nickel (Ni), copper (Cu), gold (Au), and silver (Ag) as well as the 2D semimetal graphene (Gr). Thin metal films of only three layers are used, corresponding to a full ABC stacking for the (111) fcc lattices. In the case of the same metal on each side, the structures are essentially in short-circuit boundary conditions as the metal contacts are equipotential.<sup>52</sup> Without electrodes, a transition from an antiferroelectric ground state to a ferroelectric ground state occurs at a thickness of  $\sim 10$  nm (16 layers). When the effect of electrodes is included, the ferroelectric state becomes stabilized at smaller thicknesses. Furthermore, for the conventional metal contacts (Ni, Cu, Au, and Ag), a quasi-ferroelectric (QF) structure occurs for thicknesses greater than two layers, which is lower in energy than either the FE or AFE structure and stabilizes a net polar phase. At the bilayer limit, the ferroelectric phase is stabilized by Ag metal contacts and Au metal contacts under strain. Moreover, the Au and Ag contacts lead to an enhancement of polarization as indicated by the increased Cu displacements, causing the HP state to be more favorable than the LP state. Through an analysis of the electron charge density and the projected density of states (PDOS), comparisons between two different classes of electrodes (Gr vs Au) as well as different out-of-plane ferroelectrics,  $\alpha\text{-In}_2\text{Se}_3$  and  $\text{d1T-MoTe}_2$ , indicate that interfacial bond formation leads to more subtle changes in polarization for these other layered materials. Although the PDOS indicates that the CIPS layers immediately adjacent to the electrodes are metallic through contact doping, energy-barrier calculations show that switching of these layers under an electric field is still possible. Taken together, these results show the importance of including interfacial contacts when studying ultrathin, van-der-Waals-based ferroelectrics and that these contacts can recover the ferroelectric behavior seen in bulk.

## II. METHODOLOGY

DFT calculations were performed using the Vienna *ab-initio* Simulation Package (VASP)<sup>53</sup> where the core-electron/valence-electron interactions were described via the projected-augmented-wave (PAW) method.<sup>54,55</sup> The wave functions were expanded in a plane-wave basis using a 400 eV energy cutoff. Exchange-correlation effects were described using the Perdew-Burke-Ernzerhof<sup>56</sup> generalized gradient approximation including van der Waals corrections via Grimme's DFT-D3 method with Becke-Johnson (BJ) damping.<sup>57,58</sup> Given that the space group symmetry of  $\text{CuInP}_2\text{S}_6$  (No. 9, Cc) is base-centered monoclinic, a more primitive unit cell with two formula units per cell (one per layer) can be constructed from the standard conventional cell with four formula units per cell (two per layer). For FE and alternating-layer AFE structures, particularly, with metal contacts, this unit cell is more computationally convenient to use. The structural

**TABLE I.** Lateral supercell models used for CIPS with different electrodes and their lattice mismatch (in each case the metal was strained in the stated direction to match the CIPS lattice).

Electrode	Model	Lattice mismatch (%)
Ni	$\sqrt{3} \times \sqrt{3}$ CIPS/ $4 \times 4$ Ni(111)	+5.6
Cu	$\sqrt{3} \times \sqrt{3}$ CIPS/ $4 \times 4$ Cu(111)	+2.7
Au	$1 \times 1$ CIPS/ $2 \times 2$ Au(111)	+5.4
Ag	$1 \times 1$ CIPS/ $2 \times 2$ Ag(111)	+5.0
Graphene	$2 \times 2$ CIPS/ $5 \times 5$ Graphene	-1.3
No electrode (freestanding)	$1 \times 1$ CIPS	N/A

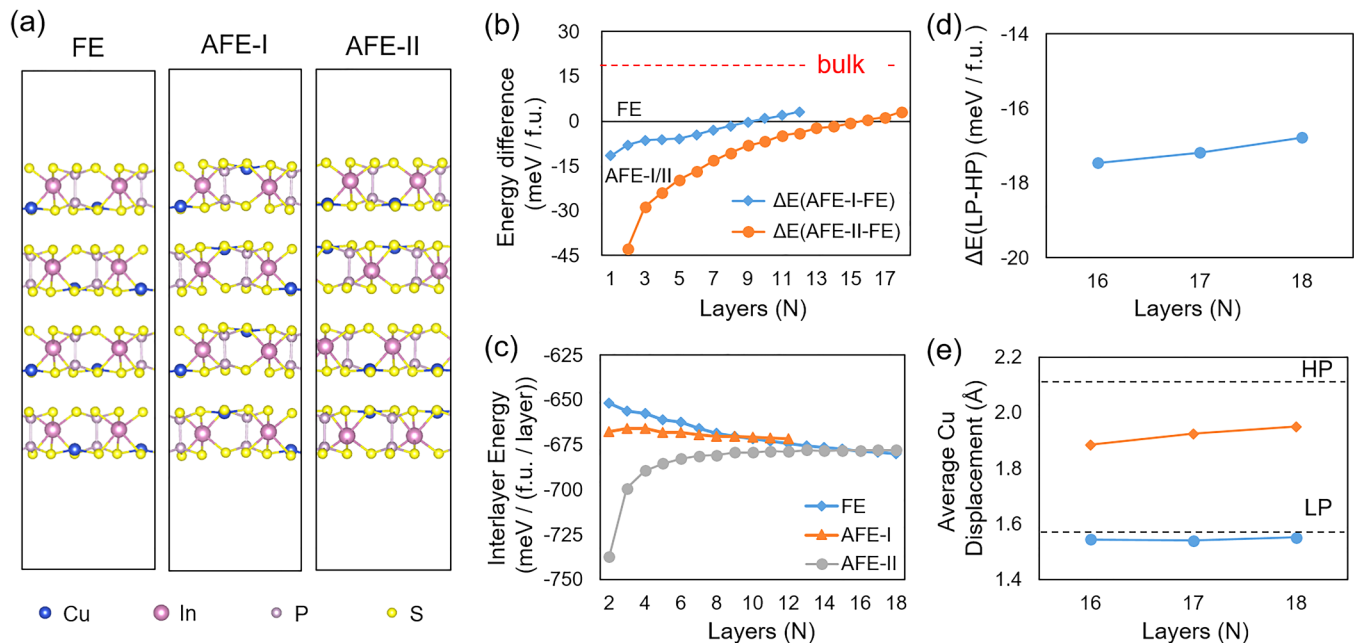
models and the corresponding lattice mismatch are described in Table I. Brillouin zone integration was performed on  $\Gamma$ -centered Monkhorst-Pack k-point grids.<sup>59</sup> Convergence tests for freestanding CIPS, using  $4 \times 4 \times 1$ ,  $6 \times 6 \times 1$ , and  $8 \times 8 \times 1$ , and for Gr/CIPS/Gr, using  $3 \times 3 \times 1$ ,  $4 \times 4 \times 1$ , and  $5 \times 5 \times 1$ , indicate that the energy differences  $\Delta E = E_{\text{AFE}} - E_{\text{FE}}$  are well converged (1–2 meV/f.u.; even better convergence for the thicker slabs). The results shown in the main text were obtained with  $6 \times 6 \times 1$  grids for freestanding CIPS and  $4 \times 4 \times 1$  for Gr/CIPS/Gr. The sampling was tested for the Au and Ag contacts using  $6 \times 6 \times 1$  through  $10 \times 10 \times 1$  and achieved a similar level of convergence. The results in the main text were obtained with  $8 \times 8 \times 1$ . For Cu and Ni, the size of the supercell had to be much larger (i.e., laterally  $3\times$  as large compared to Au and Ag) in order to accommodate a reasonable level of lattice constant mismatch. It was

not computationally practical to go beyond a  $3 \times 3 \times 1$  grid, which, however, is compensated to some level by the larger supercell. Vacuum separations of  $\sim 15$  Å were used to minimize periodic interaction of slabs along the z-axis. Electrostatic dipole corrections were used as necessary. For each structure, the in-plane lattice parameters were held fixed to those of CIPS while all atomic coordinates were fully relaxed until the net force on all was less than  $0.01$  eV/Å. The energy barriers for bilayer switching were calculated using the climbing-image nudged-elastic band (CI-NEB) method.<sup>60,61</sup> Finally, we note that in a prior work,<sup>28</sup> norm conserving pseudopotentials (NCPPs) had been used as well as the PAW method. While both methods give a quadruple well potential energy curve, the NCPP indicates the HP structure to be lower in energy by 22 meV/f.u., whereas PAW indicates the LP structure to be lower in energy by 2 meV/f.u. Although these small numbers are within the uncertainty of the exchange-correlation energies, the LP polarization is more commonly observed. The PAW method can be effectively viewed as an all-electron-derived pseudopotential, owing to the fact that the pseudo wave functions are constructed by explicit consideration of the core electrons. The better agreement of the PAW results with experimental data further validates the choice of using the PAW method for all subsequent CIPS calculations.

### III. RESULTS

#### A. Freestanding $\text{CuInP}_2\text{S}_6$

For freestanding CIPS, we consider three possible structures for our thickness dependent study, as shown in Fig. 1(a) for the

**FIG. 1.** Layer-dependent ferroelectric properties of  $\text{CuInP}_2\text{S}_6$  without electrodes. (a) Structure of four-layer CIPS with ferroelectric (FE), antiferroelectric type-I (AFE-I), and antiferroelectric type-II (AFE-II) ordering. (b) Energy difference between FE and AFE-I/II as a function of layer number. (c) Interlayer-coupling energy as a function of layer number for each ordering type. (d) Energy difference between LP and HP as a function of layer number. (e) Average Cu displacement as a function of layer number.

four-layer case. In the ferroelectric state, the Cu atoms of all layers are on the same side [the leftmost panel of Fig. 1(a)]. For antiferroelectric states, we consider structures with intralayer AFE ordering so that each layer has a net-zero dipole [labeled AFE-I in Fig. 1(a)] and structures with interlayer AFE ordering [labeled AFE-II in Fig. 1(a)]. We note that for the AFE-II type, only structures with an even number of layers have a net zero polarization; for odd numbers of layers, a small net polarization associated with one layer is present.

The present calculations, shown in Fig. 1(b), indicate that the antiferroelectric ordering is persistent up to a thickness of 16 layers (~10 nm) and that the AFE-II ordering is energetically preferred over AFE-I. In traditional, displacive ferroelectrics, the depolarizing field often forces the system into a phase where there are either no or minimal polar distortions.<sup>62</sup> However, given that the paraelectric phase of CIPS is a disordered state with Cu atoms randomly occupying sites on opposite sides of the layer with equal probability<sup>29,44</sup> and local dipoles that cancel, preferential ordering in the AFE states is not surprising as it allows for the accommodation of the depolarizing field while also maintaining the local Cu geometry of the structure. The interlayer coupling energy,  $\Delta E$ , between layers for a given thickness is calculated via

$$\Delta E = [E_{\text{multilayer}} - NE_{\text{monolayer}}]/(N - 1),$$

where  $E_{\text{multilayer}}$  and  $E_{\text{monolayer}}$  are the total energies of the  $N$  layer structure and FE monolayer structure, respectively. As shown in Fig. 1(c), after 10 layers for AFE-I and 16 layers for AFE-II, the ferroelectric interlayer coupling becomes stronger than the antiferroelectric coupling indicative of the stabilization of ferroelectric ordering.

As mentioned in earlier papers,<sup>28,63</sup> the HP configuration for CIPS can be stabilized due to compressive strain or the local environment in the material. For a finite ferroelectric CIPS slab, the outward facing Cu atoms in the surface layer can only be in an LP-like coordination because the HP state requires the presence of another layer to enable the Cu atoms to bond to S atoms in that layer. In principle, all other layers can be in either polarization state. However, due to the larger polarization of the HP phase and consequently its larger depolarization field, the HP phase cannot be stabilized below 16 layers. Energetically, at this limit, the energetic favorability LP phase is significantly larger than for bulk structures [Fig. 1(d)]. Furthermore, the atoms of the LP state are, on average, slightly closer to the centrosymmetric position, suggesting a remnant depolarizing effect [Fig. 1(e)]. Likewise, for the HP state, there is a stronger depolarizing effect partially due to the two inward facing surface layers remaining in an LP-like state at the considered thicknesses.

## B. Metal-contact stabilization

For the inclusion of contacts, we first compare the freestanding bilayer CIPS to heterostructures consisting of bilayer CIPS with Gr, Ni, Cu, Au, or Ag contacts. The optimized structures are shown in Fig. 2(a). Most remarkably, the Ag contact stabilizes a high-polarization FE state. Just like in the freestanding case, the bilayer remains in an inward-facing AFE-II configuration (where

Cu atoms in the interfacial layers are at the inner layer edges) when the contacts are Gr, Ni, or Cu. On the other hand, for the Au case, an outward-facing AFE-II configuration (where Cu atoms in the interfacial layers are at the outer layer edges) is preferred in the ground state with displacements between that of the typical LP and HP displacement values. For the Gr case, the CIPS layers remain mostly unperturbed and the Cu atoms remain in almost the same relative position, as shown in Fig. 2(b), since the Gr and CIPS bonding is solely via van der Waals interactions. In contrast, for both Ni and Cu contacts, the structural framework of CIPS becomes very distorted as a result of strong interactions between the sulfur atoms and the metal layers. The distortion of the framework leads to a decrease in the Cu displacements relative to the freestanding and Gr cases for Ni, while the shifts in displacement average out for the Cu contact. Compared with Ni, the difference in adsorption energy between S and Cu is smaller for Ag and Au, indicating that Cu can more readily interact with these metals [see Fig. 3(a)]. Such a trend aligns with experimental observations for the relative affinity of metals to interact with sulfur.<sup>64</sup> It is most notable that Ag and Au metallic layers on bilayer CIPS lead to different preferred ordering by a significant amount of energy difference. However, it has not been possible to trace the origin of this effect.

The layer-dependent trend for FE vs AFE ordering is shown in Fig. 2(c). In all cases, FE ordering is stabilized with fewer layers than in the case of freestanding CIPS. For the case of graphene electrodes, the AFE to FE transition occurs when the thickness surpasses four layers. Although such a behavior is counterintuitive given the lack of direct bonding at the Gr/CIPS interface, a strong electrostatic interaction exists between the Gr and CIPS as illustrated by the projected density of states in Figs. 3(b) and 3(c). Comparing a thickness increase in the FE state from the bilayer case to the six-layer case, shifts in the Fermi energy relative to the Dirac point of graphene lead to increased metallicity and, hence, a change in screening from the Gr. Given the van der Waals nature of the interface between CIPS and Gr, the interfacial strain may be slightly different than that assumed in the calculation. In such a case, there would be a small change in the Gr Fermi velocity for all thickness cases and the trend in the screening behavior overall would remain essentially unchanged.

For the Ni electrode, a low-energy interfacial atomic arrangement occurs when each of the Cu atoms of the CIPS interfacial layers aligns with a Ni atom in each of the layers of the contact. In fact, this interfacial arrangement is the only that supports a metastable ferroelectric phase at the bilayer limit (155.2 eV higher in energy than the AFE state). In the other interfacial stacking configurations tested, the interfacial distortions always lead to the creation of an AFE state under structural relaxation. Calculation of the thickness dependence of the relative energy beyond 10 layers of CIPS with Ni becomes computationally prohibitive; however, extrapolation of the trend in Fig. 2(c) (solid green line, diamonds) implies stabilization of the FE phase around 12–14 layers of CIPS. As shown in the atomistic structures of Fig. 4, even as the layer thickness increases, the large distortions in the interfacial layers persist and, for the FE solution, some copper atoms relax to the opposite side of the interface. Such distortions have been observed in calculations of Ni/CIPS interfaces utilizing other geometries.<sup>63</sup>



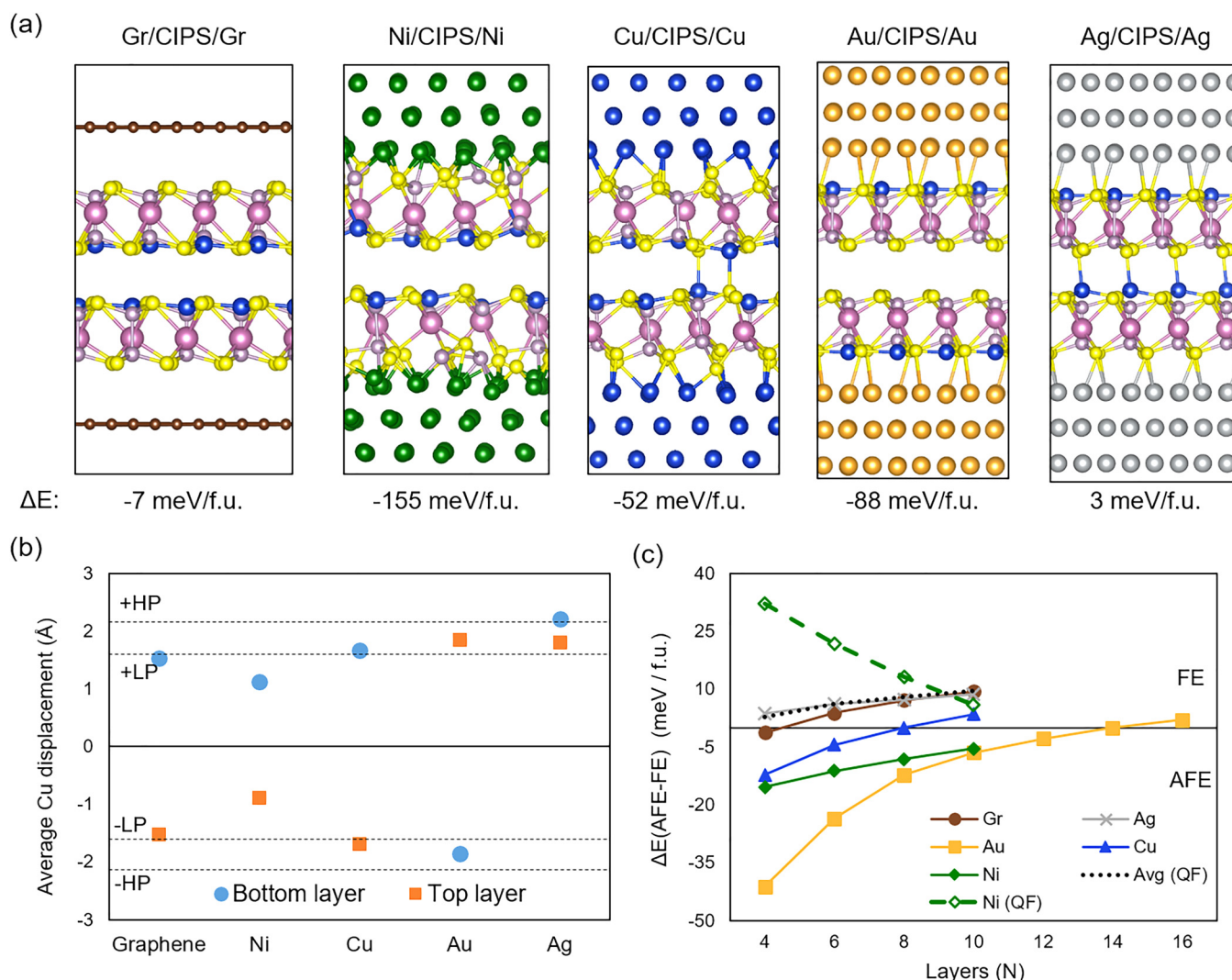


**FIG. 2.** (a) Structure of bilayer CIPS with different electrodes: graphene (Gr), nickel (Ni), copper (Cu), gold (Au), and silver (Ag), respectively. The relative energy between AFE and FE states ( $\Delta E = E_{\text{AFE}} - E_{\text{FE}}$ ) is shown below each lowest energy bilayer structure. (b) Average Cu displacement in the bottom and top layers for each system. The dashed lines reference the atomic displacements for the  $\pm$ LP and  $\pm$ HP states in bulk CIPS. (c) Energy difference between FE and AFE-II-type as a function of layer number (negative indicates AFE is preferred). In addition, the dashed lines indicate the relative energies for the quasi-ferroelectric structures discussed in the main text.

Therefore, we consider a novel structure that we term a quasi-ferroelectric (QF) state in which the interfacial layers orient themselves in their preferred geometry while the internal layers are ferroelectric (see the right hand side of Fig. 4). Essentially for  $N$  layers of CIPS, this can be thought of as  $N - 2$  FE layers with a bilayer of AFE. Such a structure is found to be the overall lowest energy of the considered structures starting with four-layer CIPS and leads to the stabilization of a net polar structure in all but the bilayer case [dashed green line, diamonds in Fig. 2(c)]. Furthermore, the existence of an inward facing, orientation opposing layer may explain

why significant time/voltages are needed to initiate electroplating under ionic conductivity of CIPS with Ni electrodes.<sup>63</sup>

For the Cu electrode (where the metal aligns over the Cu sites in the CIPS), increasing the thickness of CIPS to eight layers stabilizes the FE phase compared to the  $\sim 12$  layers with Ni. Taken together, this suggests a competing role between the stabilization of the FE phase and the interfacial chemical interactions at metal-CIPS interfaces. For Ag, the ferroelectric phase was already favored in the ground state at the bilayer case and little change is seen as a function of thickness. For Au, the preference of the outward facing Cu

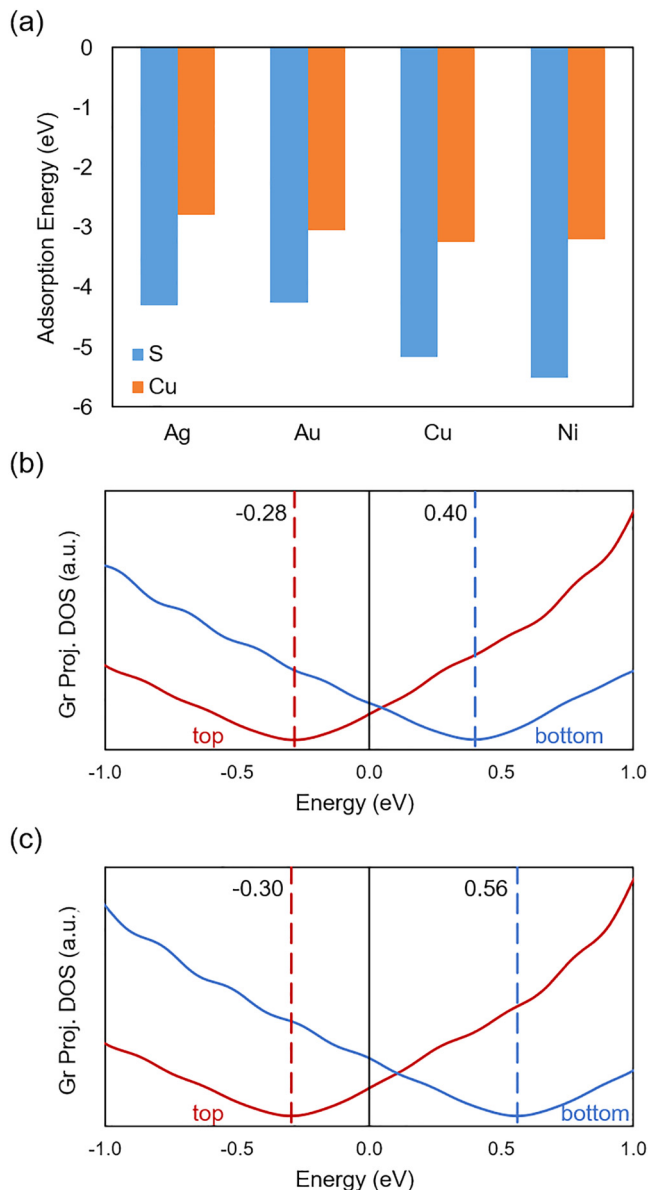


**FIG. 3.** (a) Adsorption energies for sulfur and copper on different substrates. (b) Partial density of states projected on graphene for bilayer ferroelectric CIPS. (c) Partial density of states project on graphene for six-layer ferroelectric CIPS. For (b) and (c), top and bottom are defined for CIPS with an upward polarization so that the top (red) layer is adjacent to the side of CIPS with Cu atoms at the edge and vice versa for the bottom (blue) layer.

displacements leads the AFE being favored until just past 12 layers. Overall, the interaction between the ferroelectric material and metal electrode dominates the overall behavior when CIPS has a thickness of only a few layers and decays as the CIPS becomes thicker.

Motivated by the presence of the QF state for the Ni contacts, we additionally considered such a state for the Cu, Au, and Ag

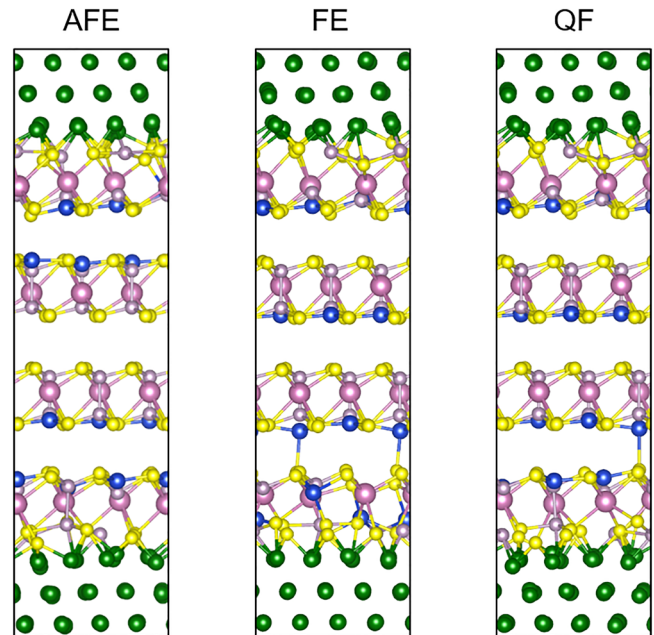


**FIG. 4.** Comparison of the optimized structure for four layers of CIPS with Ni in the antiferroelectrics (AFE), ferroelectric (FE), and quasi-ferroelectric (QF) structures.

electrodes. In each case, the layers at the interface behave the same as in the bilayer case while still obeying the general  $N - 2$  ferroelectric/bilayer antiferroelectric behavior discussed for Ni. That is to say, for Au and Ag contacts, the Cu atoms in the interfacial layers still reside on the sides of the CIPS layers closest to the contact whereas for the Cu contacts, they reside on the sides of the CIPS layers furthest from the contact. Despite this difference, all three contacts favor the quasi-ferroelectric state in comparison to the ferroelectric or antiferroelectric state and the general energetic trend is the same for all three of these contacts. Furthermore, their specific relative energies are within uncertainty of each other. Therefore, we only plot the average of this trend in Fig. 2(c) (the dashed black line). We note that this energy trend is quite similar to that for the Ag ferroelectric comparison. In fact, while the QF solution results in a significant departure from the ferroelectric solution trend in Cu and Au, the Ag-specific data only slightly favor the QF solution.

### C. Boundary clamping and strain effects

In the cases of the Au and Ag contacts, the ability to, under strain, lattice match with small commensurate orderings leads to several interesting possibilities for interfacial engineering. First, within the lateral xy-plane, the  $P_2S_6$  columns (in which the Cu displace) can be aligned with the Au or Ag contact at either a top site (Au/Ag in the interfacial layer), face-center-cubic site (Au/Ag in the second layer), or hexagonal-close-packed site (Au/Ag in the third layer). For brevity, we hereafter refer to these as top site, fcc site, and hcp site, respectively. For the systems considered here,

alignment with the top site is the global minimum in energy. However, if we strip away a layer of metal, the fcc site becomes the global minimum in energy. This indicates that careful considerations during device heterostructure fabrication may be used to tune the interfacial structure. The hcp site was found to always be significantly higher in energy.

Given this consideration, in Fig. 5(a), we expand upon the calculations shown in Fig. 2 to include comparisons of the FE and AFE energies at the fcc site and top site for both Au and Ag. As before, the inward facing AFE structure is always higher in energy than the outward facing AFE structure for these contacts and therefore not shown. For the case of Ag, switching from the top site to the fcc site destabilizes the FE solution and now the system favors AFE ordering for the bilayer and four-layer cases. For Au, on the other hand, there is an increase in the relative stability of the FE solution and ferroelectricity becomes preferred at 8 layers as opposed to the 14 layers for the top site. Again, for thicknesses beyond the bilayer, a quasi-ferroelectric solution exists for the shifted geometries. When considering this QF structure, again very little difference is found between Au and Ag as well as between top and fcc sites within uncertainty and this trend is shown as a single dashed black line in Fig. 5(a).

It should be noted that the outward facing AFE solution has an overall expanded lattice compared with the FE solution.

Focusing on the bilayer, the AFE stack for Au is  $\sim 0.3$  Å ( $\sim 1.3\%$ ) thicker at both the fcc site and top sites. In silver, the AFE stack at the fcc site is  $\sim 0.1$  Å ( $\sim 0.5\%$ ) thicker. Owing to this difference as well as the known sensitivity of CIPS phases to strain,<sup>28,42,65,66</sup> in Fig. 5(b), we explore the energetic behavior of first clamping the bilayer stacks to the FE boundary conditions and then the application of additional compressive strain. For the Au top site stack, although the relative stability of the AFE solution decreases, it remains the preferred state over the considered range of strains. For the Au fcc site stack, whose AFE and FE structures are shown in Fig. 5(c), the initial clamping decreases the relative stability of the AFE solution and under additional compressive strain leads to stabilization of the FE solution at 1% strain. For the Ag fcc site stack, since the clamping is less significant than in the Au stack, the initial shift in the AFE stability is much less pronounced and stabilization of the FE solution occurs at  $\sim 1.5\%$  compressive strain.

#### D. Interfacial effects and contact doping

In order to further investigate the effect of the electrode and its interface on the outer most layers of CIPS, we analyze the average Cu displacement in each layer for a 10-layer CIPS structure in Fig. 6. This thickness was chosen since there is an interface geometry supporting a ferroelectric solution for each of graphene,

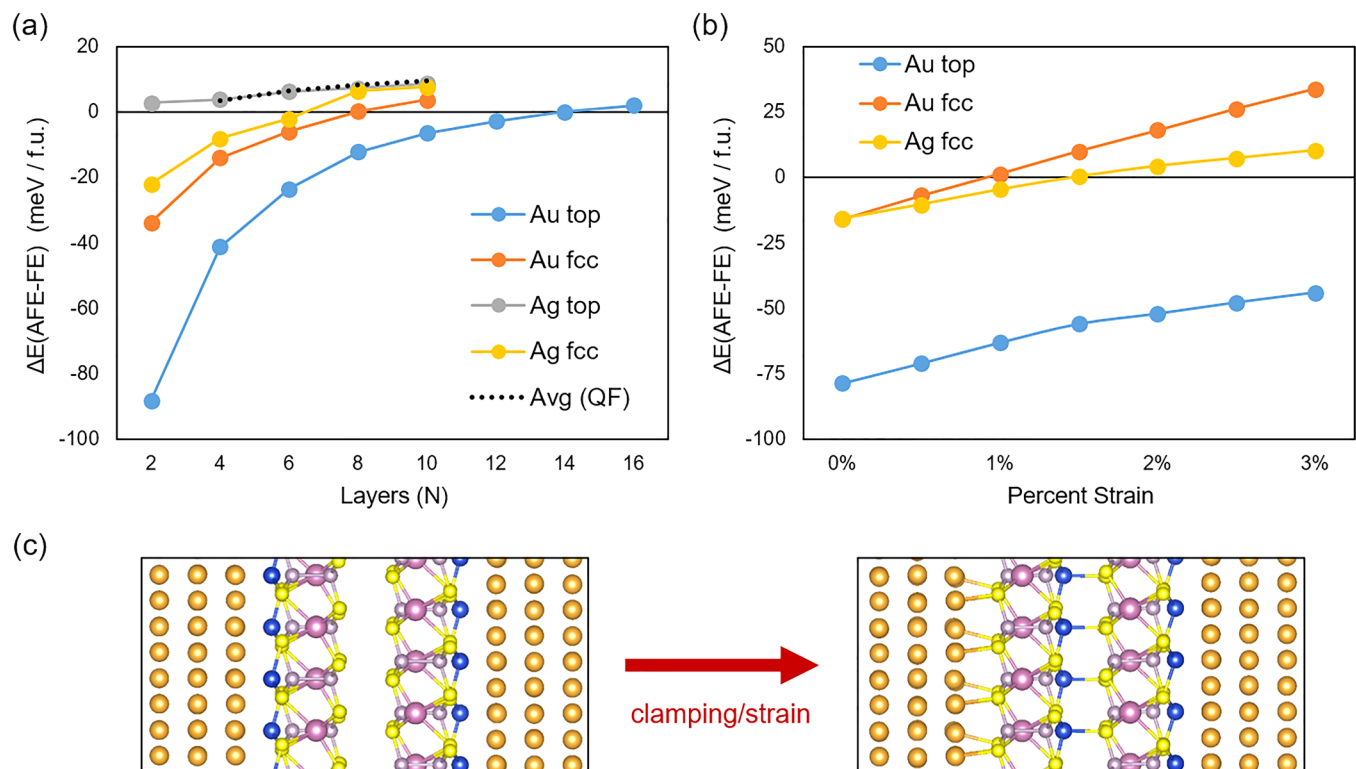


**FIG. 5.** (a) Stacking dependence of the relative energies for AFE vs FE for both Au and Ag contacts. The average over all quasi-ferroelectric solutions is shown as well. (b) FE stabilization effect as a function of compressive strain on clamped bilayer structures. (c) Atomistic structure of bilayer CIPS with Au contacts in the outward facing AFE and stabilized FE states. In both cases, Cu atoms favor locally HP site positions.



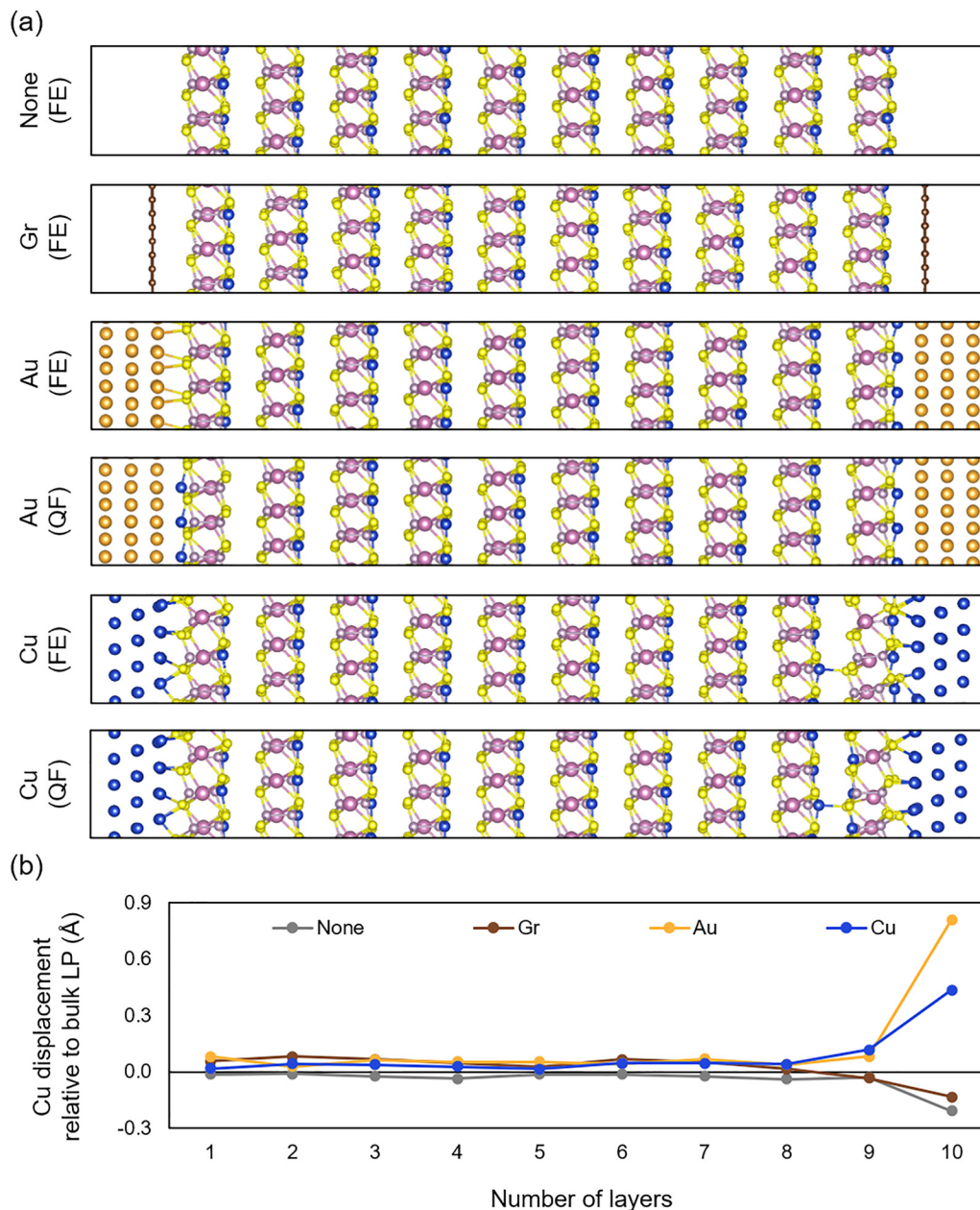


**FIG. 6.** (a) Structure of 10-layer ferroelectric CIPS with no contact and with graphene, Au (both ferroelectric and quasi-ferroelectric), and Cu electrodes (both ferroelectric and quasi-ferroelectric), respectively. (b) Average Cu displacement relative to the bulk LP position in each layer for each of the ferroelectric structures in (a).

Cu, and Au (fcc). Although the 10-layer freestanding CIPS is not ferroelectric in its ground state, it is still informative to use this structure as a point of comparison. Using the average distortion as a stand-in for the polarization,<sup>52</sup> we can infer how differing layer-by-layer distortions throughout the slab add or cancel to

contribute to the overall observable polarization and also make comparisons to bulk calculations.

Without the electrodes, the Cu displacements are slightly smaller than in the bulk with the exception of the top layer where they are significantly smaller. Overall, the average Cu displacements

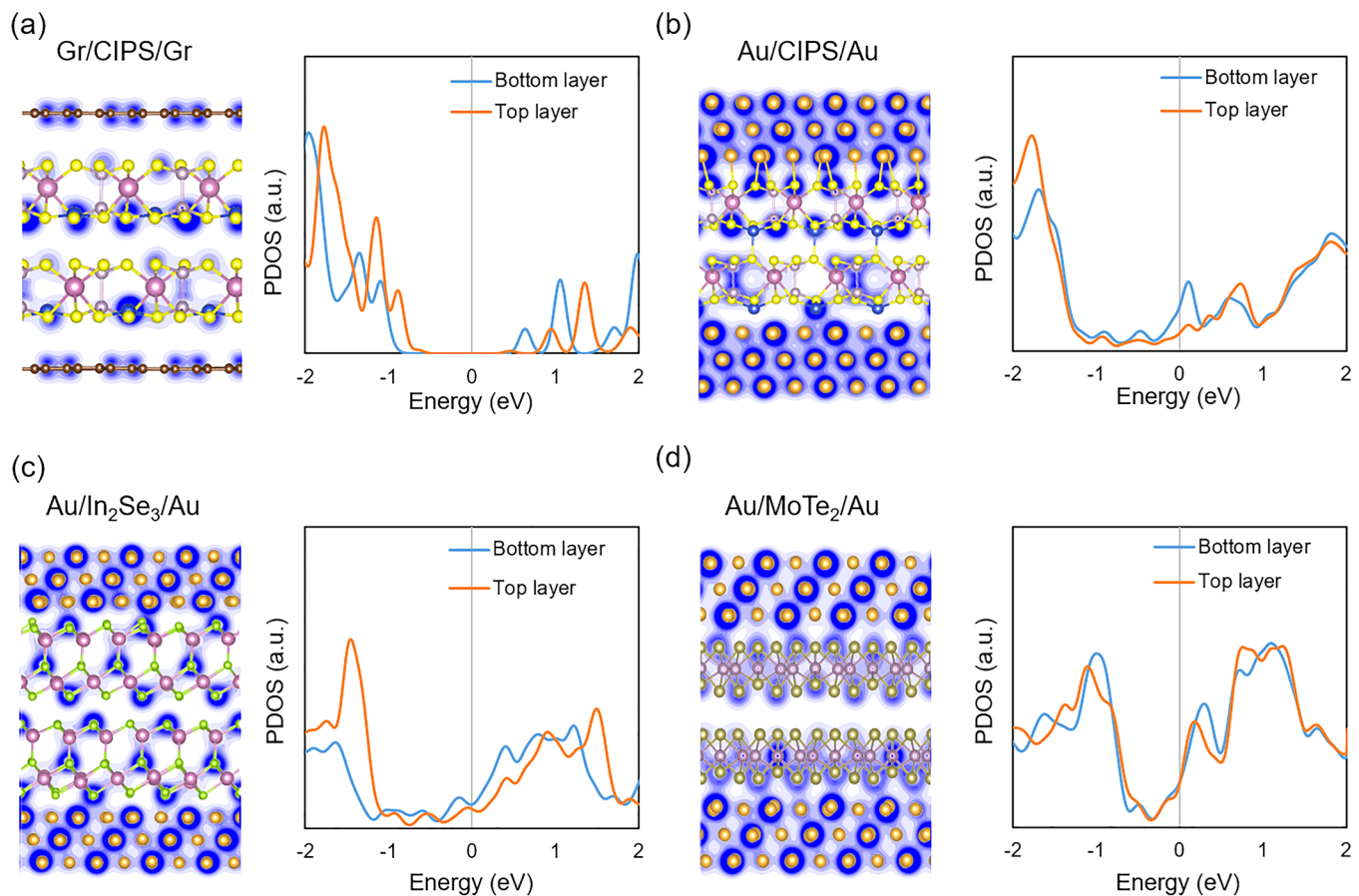


**FIG. 7.** Electron charge density contour and projected density of states (PDOS) in bilayer 2D ferroelectric materials with electrodes. Top and bottom layers for the PDOS refer only to the ferroelectric layers and the metal contact PDOS are not shown. (a) Bilayer CIPS with graphene electrodes. (b) Bilayer CIPS with Au electrodes. (c) Bilayer  $\alpha$ - $\text{In}_2\text{Se}_3$  with Au electrodes. (d) Bilayer d1T-MoTe<sub>2</sub> with Au electrodes.

in the 10-layer freestanding structure are slightly smaller ( $-2.6\%$ ) than the bulk LP Cu displacements ( $1.57 \text{ \AA}$ ) because of the presence of the depolarizing field. In the case of graphene contacts, displacement of the Cu atoms facing graphene is still suppressed, but less than in the freestanding case. The middle layer and bottom layers are slightly enhanced. This result suggests that graphene can partially screen the depolarization field after a few layers and the overall average Cu displacement is  $0.024 \text{ \AA}$  ( $1.5\%$ ) larger than the bulk LP. For the Cu and Au electrodes, despite their differing interfacial geometries and the larger interfacial distortions in the former, both have an overall increase in the CIPS Cu displacements throughout the structure. This is most pronounced at the interface with the Au contact having a more significant effect. For the Au electrode, the effect is caused by the Cu displacing toward the fcc surface site. For the Cu electrode, while some of the Cu can displace toward surface voids, the large distortion of the CIPS layer also pushes back some of the dimers as the sulfur atoms are pulled more strongly toward the Cu surface than for the Au surface. The average increases

in relative displacements for the structures are  $0.082 \text{ \AA}$  ( $5.2\%$ ) and  $0.13 \text{ \AA}$  ( $8.3\%$ ), respectively. When considering the quasi-ferroelectric structure for Cu and Au [shown schematically in Fig. 6(a) alongside their fully FE counterparts], although enhancements of the local layer dipoles do occur for the inner layers, the concept of an average increase in displacements is no longer as helpful due to the counteracting layer. Instead, a comparison of the overall average displacement is more informative. For the Au electrode, the overall average displacement in the FE case is  $1.70 \text{ \AA}$ , whereas for the QF case it decreases to  $1.29 \text{ \AA}$  representing a decrease in the remnant polarization by  $18\%$  compared to bulk. Similar values for the QF case occur for the Cu electrode as well.

Since clamping stabilizes ferroelectricity for Au with an fcc interface as discussed in Sec. III C, we analyzed the change in the average Cu displacement for different thicknesses of CIPS with the Au metal contact. As previously indicated in Fig. 5(c), the bilayer distortion becomes similar to that of the bulk HP phase. In general, for this interface, the displacements are enhanced more

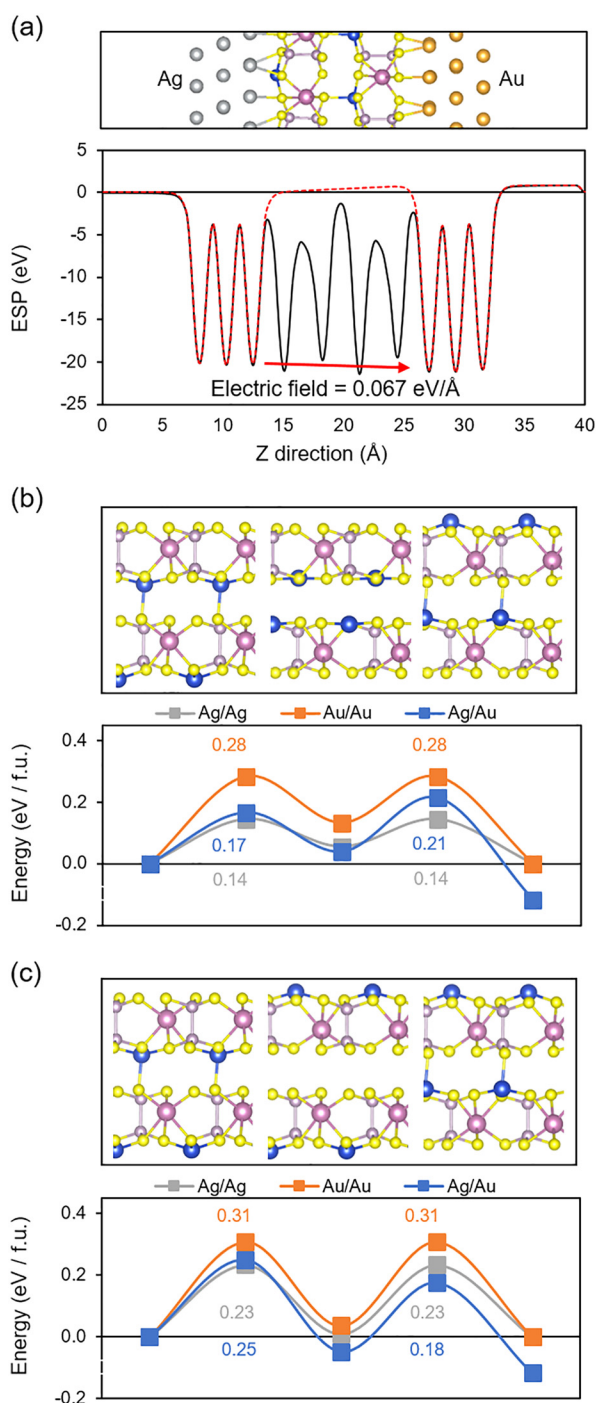


**FIG. 8.** Ferroelectric switching in bilayer CIPS with electrodes. (a) Atomistic model and electrostatic potential (Ag side set to zero) to approximate the effects of an electric field. (b) Energy barriers for ferroelectric switching (per Cu atom) through an inward facing AFE intermediate for Ag/Ag, Au/Au, and Ag/Au contacts. (c) Energy barriers for ferroelectric switching (per Cu atom) through an outward facing AFE intermediate for Ag/Ag, Au/Au, and Ag/Au contacts.

significantly as the CIPS layer becomes thinner. While at 8-layers, the average displacement is similar to that of the 10-layer structure, increasing only by 0.03 Å. An enhanced HP state is stabilized at six and fewer layers. In bulk, the HP state has an average Cu displacement of 2.14 Å; however, for six layers of CIPS, the displacement is 2.18 Å and the displacement increases to 2.28 Å in the bilayer case. Overall, these trends suggest that metal contact choice and interface effects have a significant impact not just on stabilizing ferroelectricity but also on the slab's polarization at the ultrathin limit.

While local layer enhancements still occur for the QF structure, decreasing thickness of the CIPS region leads to a significant decrease in the net polarization for the QF structure. The severity of the decrease in observed polarization with decreasing thickness can be approximated as a reduction in the average dipole of the slab by  $\frac{2}{N}$  for  $N$  layers and reaches a nominal 50% decrease in the limit of four-layer CIPS neglecting any local enhancement of the layers that remain ferroelectric. For the Au with an fcc interface, the decreased average polarizations across the slab for the 8- through 4-layer cases are 1.19 Å (−24%), 1.06 Å (−32%), and 0.80 Å (−49%), respectively. These values are slightly less than the nominal reduction due to the effects of small local enhancements that remain in the layers.

In order to better understand the role of the polarization enhancement by metal contacts, we analyze the electron charge density and projected density of states (PDOS) for bilayer CIPS with both Gr and Au contacts when CIPS is in the ferroelectric state. Furthermore, we include an analysis of two other ferroelectric bilayers with out-of-plane polarization,  $\alpha$ -In<sub>2</sub>Se<sub>3</sub> and d1T-MoTe<sub>2</sub>. In the case of the graphene electrodes with CIPS [Fig. 7(a)], there is only weak van-der-Waals bonding between the graphene layers and CIPS layers and the CIPS layers remain insulating (the shift between band edges arises from the internal, dipole-induced electric field). However, for the Au electrodes, all three ferroelectrics become metallic. As exemplified by the PDOS, this contact doping is not caused by band alignment between the metal Fermi energy and the insulating ferroelectrics, but rather there is now non-zero PDOS where the bandgaps were. From the electron charge density contour maps, we can see that this occurs because of the formation of bonds between Au and S or Cu in CIPS [Fig. 7(b)], Au and Se for  $\alpha$ -In<sub>2</sub>Se<sub>3</sub> [Fig. 7(c)], and Au and Te for d1T-MoTe<sub>2</sub>. In  $\alpha$ -In<sub>2</sub>Se<sub>3</sub>, bonding of Au to the outer most Se layer leads to a stretching of the  $\alpha$ -In<sub>2</sub>Se<sub>3</sub> layers and causes an increase in the distance of the middle Se atom from its centrosymmetric point. This enhancement occurs more so in the lower layer than in the upper layer of Fig. 7(c) (0.53 and 0.48 Å, respectively, vs 0.46 Å in the contact-free bilayer; increases of ~18% and 6%, respectively). This enhancement of polarization is in contrast to the effect that graphene has on  $\alpha$ -In<sub>2</sub>Se<sub>3</sub><sup>26</sup> and due to the formation of stronger bonds between the contact and  $\alpha$ -In<sub>2</sub>Se<sub>3</sub>. In contrast, we find a very slight depolarizing effect in the d1T-MoTe<sub>2</sub> structure [Fig. 7(d)]. For bilayer d1T-MoTe<sub>2</sub>, an asymmetry in the trimer bond lengths is present in both the freestanding and Au-contact structures. In the lower layer, the trimer bond lengths increase by ~1% and in the upper layer, they increase by ~0.1%. The upper layer also develops a slight asymmetry to the trimer itself. In general, CIPS has the largest enhancement of polarization due to the ability for the ferroelectric-responsible atom (Cu) to directly bond with the metal contact.



Enhancement, rather than suppression, of the polarization due to the bonding geometry between the ferroelectric and contact is similar to the BaO-terminated BaTiO<sub>3</sub> interface with Pt which does not occur for other terminations.<sup>16</sup> For typical vdW ferroelectric materials, the surface termination, on the other hand, is (up to a polarization direction dependence) fixed and the strength of contact bonding may strain the material. CIPS has the added uniqueness that the atom responsible for the ferroelectricity is significantly more mobile and sits at the surface rather than being embedded within the layer and can thus more readily interact with the contacts.

### E. Bilayer switching pathways

Finally, we consider the ability for the contact-stabilized ferroelectric bilayer CIPS to switch from one polarization direction to the other. We consider three different combinations of electrodes: Ag/Ag, Au/Au, and Ag/Au. In keeping with the results of Sec. III C, we use structures that have been first clamped to the ferroelectric solution and strain stabilized with 2% compressive strain so that FE ordering is robustly preferred in all cases. The use of asymmetric contacts (Ag/Au) provides a means to include an electric field in the calculation given the different work functions of the metals. Although a real device constructed in such a way would be expected to have an asymmetry in the P-E loops due to the additional internal electric field (along the lines of Ref. 63), we stress that this is primarily a computational construct since an external field cannot directly be applied in the presence of metal contacts in our calculations.

Calculations of the electrostatic potential [Fig. 8(a)] indicate that such an arrangement provides an equivalent 0.067 eV/Å electric field across the material. If the thickness of CIPS were increased, such an electric field would decrease linearly with separation of the asymmetric contacts. For each of the sets of contacts, we consider two different simplified pathways: (1) switching through an inward AFE intermediate as shown in Fig. 8(b) and (2) switching through an outward AFE intermediate as shown in Fig. 8(c). In these pathways, for simplicity, the Cu atoms within a layer move in a concerted fashion, but the two layers switch independently of each other. Due to the order-disorder nature of CIPS, such an approximation provides a way to allow for some increased degrees of freedom of the Cu atoms. In thicker systems, the motion may become significantly more complicated. For symmetric Ag/Ag contacts, pathway 1 has a lower overall barrier (despite the higher energy of intermediate inward AFE state compared to the outward AFE state). For symmetric Au/Au contacts, pathway 2 has a lower barrier. In the case of the asymmetric Ag/Au contacts, a polarization state with the Cu atoms on the Au side is the ground state and the overall barrier for pathway 2 is favored. Furthermore, for this pathway, the energy of the intermediate AFE state is between that of starting and ending FE states indicating a continued driving force from one FE state to the other by the electric field induced by the asymmetry.

### IV. CONCLUSIONS

In summary, the effect of various metal contacts on 2D ferroelectrics which have out-of-plane polarization, with a primary

focus on CuInP<sub>2</sub>S<sub>6</sub>, was investigated using DFT calculations. For CIPS, the monolayer is antiferroelectric within the plane due to the presence of a depolarizing field and the material's order-disorder nature. Without electrodes, there is a layer-dependent transition from an interlayer AFE ordering to FE ordering when the thickness is larger than ~10 nm (16 layers). At the bilayer limit for CIPS, the system remains antiferroelectric for graphene, Ni, Cu, and Au electrodes; however, CIPS becomes ferroelectric at this thickness for Ag electrodes. Additionally, a quasi-ferroelectric structure exists for the conventional metal contacts which stabilizes a polar structure down to at least the four-layer limit due to a combination of increased metallic screening from the contact doping of these layers and a smoothing of the structural distortions for the interior layers. The presence of such a quasi-ferroelectric structure indicates that ultrathin CIPS structures may exhibit partial switching behaviors and lower than expected remnant polarizations. Furthermore, interfacial engineering and strain can be used to stabilize ferroelectricity at the bilayer limit with Au electrodes and Ag electrodes with differing geometries. In general, the critical thickness for the AFE-FE transition is much smaller than for the freestanding case without electrodes. Moreover, we find that for Au and Ag contacts, interfacial interactions between the CIPS and the metal contact lead to an overall enhancement of the polarization of the structure toward the high-polarization state of CIPS when in the ferroelectric state. A similar effect occurs for Au contacts with  $\alpha$ -In<sub>2</sub>Se<sub>3</sub>, although to a lesser extent, while d1T-MoTe<sub>2</sub> undergoes a slight depolarization. Electron charge density contours and projected density of states plots show that the outer-most layers in contact with the electrodes become metallic due to contact doping. However, reaction barrier calculations indicate that ferroelectric switching can still occur. Taken together, these results demonstrate the importance of metal contact choice and interfacial design at the ultrathin limit for 2D vdW ferroelectrics and provide insight into choices that can enhance the desired ferroelectric behavior.

We close by noting that we have presented theoretical predictions for a large number of cases of multilayer CIPS with different metals. Currently, there exist no reports of experiments on such structures to enable validation of any of the predictions. There are uncertainties in some of the details of the predictions that may arise from the choice of the exchange-correlation functional and computational necessities. The fact that the exchange-correlation functional has been used for both predictive and explanatory calculations of CIPS properties quite successfully<sup>28,31,32,63,65,66</sup> lends credence to the present predictions. The predictions made here may well motivate further experimental and theoretical research in this area.

### ACKNOWLEDGMENTS

The work at Vanderbilt University (A.O., L.T., and S.T.P.) was supported by the U.S. Department of Energy, Office of Science, Basic Energy Sciences, Division of Materials Science and Engineering under Grant No. DE-FG02-09ER46554 and by the McMinn Endowment at Vanderbilt University. L.T. was partially supported by the K. C. Wong Education Foundation of the Chinese Academy of Sciences. Computational support was provided by the National Energy Research Scientific Computing Center (NERSC), a



DOE Office of Science User Facility supported by the Office of Science of the U.S. Department of Energy under Contract No. DE-AC02-05CH11231 and also by the Department of Defense High Performance Computing Modernization Program (HPCMP). P.M., S.N., and N.B. were supported by the U.S. Department of Energy (DOE), Office of Science, Basic Energy Sciences, Materials Sciences and Engineering Division and the Center for Nanophase Materials Sciences (CNMS), which is a US Department of Energy, Office of Science User Facility at Oak Ridge National Laboratory.

## AUTHOR DECLARATIONS

### Conflicts of Interest

The authors have no conflicts to disclose.

### Author Contributions

**Andrew O'Hara:** Conceptualization (equal); Data curation (equal); Formal analysis (equal); Supervision (equal); Writing – original draft (equal); Writing – review & editing (equal). **Lei Tao:** Conceptualization (equal); Data curation (equal); Writing – original draft (equal). **Sabine M. Neumayer:** Conceptualization (equal). **Petro Maksymovych:** Conceptualization (supporting). **Nina Balke:** Conceptualization (equal). **Sokrates T. Pantelides:** Conceptualization (equal); Funding acquisition (equal); Project administration (equal); Supervision (equal); Writing – original draft (equal); Writing – review & editing (equal).

### DATA AVAILABILITY

The data that support the findings of this study are available from the corresponding author upon reasonable request.

## REFERENCES

- <sup>1</sup>V. Garcia and M. Bibes, "Ferroelectric tunnel junctions for information storage and processing," *Nat. Commun.* **5**, 4289 (2014).
- <sup>2</sup>Z. Wen and D. Wu, "Ferroelectric tunnel junctions: Modulations on the potential barrier," *Adv. Mater.* **32**, 1904123 (2019).
- <sup>3</sup>X. Wang and J. Wang, "Ferroelectric tunnel junctions with high tunnelling electroresistance," *Nat. Electron.* **3**, 440 (2020).
- <sup>4</sup>H. Cheng, J. Ouyang, Y.-X. Zhang, D. Ascienzo, Y. Li, Y.-Y. Zhao, and Y. Ren, "Demonstration of ultra-high recyclable energy densities in domain-engineered ferroelectric films," *Nat. Commun.* **8**, 1999 (2017).
- <sup>5</sup>B. Peng, Q. Zhang, X. Li, T. Sun, H. Fan, S. Ke, M. Ye, Y. Wang, W. Lu, H. Niu, J. F. Scott, X. Zeng, and H. Huang, "Giant electric energy density in epitaxial lead-free thin films with coexistence of ferroelectrics and antiferroelectrics," *Adv. Electron. Mater.* **1**, 1500052 (2015).
- <sup>6</sup>T. M. Shaw, S. Troler-McKinstry, and P. C. McIntyre, "The properties of ferroelectric films at small dimensions," *Annu. Rev. Mater. Sci.* **30**, 263 (2000).
- <sup>7</sup>D. D. Fong, G. B. Stephenson, S. K. Streiffer, J. A. Eastman, O. Auciello, P. H. Fuoss, and C. Thompson, "Ferroelectricity in ultrathin perovskite films," *Science* **304**, 1650, (2004).
- <sup>8</sup>M. D. Glinchuk, B. Y. Zaulychyn, and V. A. Stephanovich, "Depolarization field in thin ferroelectric films with account of semiconductor electrodes," *Ferroelectrics* **316**, 1 (2005).
- <sup>9</sup>S. V. Kalinin, Y. Kim, D. D. Fong, and A. N. Morozovska, "Surface-screening mechanisms in ferroelectric thin films and their effect on polarization dynamics and domain structures," *Rep. Prog. Phys.* **81**, 036502 (2018).
- <sup>10</sup>P. Gao, C. T. Nelson, J. R. Jokisaari, S.-H. Baek, C. W. Bark, Y. Zhang, E. Wang, D. G. Schlom, C.-B. Eom, and X. Pan, "Revealing the role of defects in ferroelectric switching with atomic resolution," *Nat. Commun.* **2**, 591 (2011).
- <sup>11</sup>N. Sai, A. M. Kolpak, and A. M. Rappe, "Ferroelectricity in ultrathin perovskite films," *Phys. Rev. B* **72**, 020101 (2005).
- <sup>12</sup>G. Gerra, A. K. Tagantsev, N. Setter, and K. Parlinski, "Ionic polarizability of conductive metal oxides and critical thickness for ferroelectricity in BaTiO<sub>3</sub>," *Phys. Rev. Lett.* **96**, 107603 (2006).
- <sup>13</sup>M. F. Chisholm, W. Luo, M. P. Oxley, S. T. Pantelides, and H. N. Lee, "Atomic-scale compensation phenomena at polar interfaces," *Phys. Rev. Lett.* **105**, 197602 (2010).
- <sup>14</sup>D. A. Tenne, P. Turner, J. D. Schmidt, M. Biegalski, Y. L. Li, L. Q. Chen, A. Soukiasian, S. Troler-McKinstry, D. G. Schlom, X. X. Xi, D. D. Fong, P. H. Fuoss, J. A. Eastman, G. B. Stephenson, C. Thompson, and S. K. Streiffer, "Ferroelectricity in ultrathin BaTiO<sub>3</sub> films: Probing the size effect by ultraviolet Raman spectroscopy," *Phys. Rev. Lett.* **103**, 177601 (2009).
- <sup>15</sup>P. Gao, Z. Zhang, M. Li, R. Ishikawa, B. Feng, H.-J. Liu, Y.-L. Huang, N. Shibata, X. Ma, S. Chen, J. Zhang, K. Liu, E.-G. Wang, D. Yu, L. Liao, Y.-H. Chu, and Y. Ikuhara, "Possible absence of critical thickness and size effect in ultrathin perovskite ferroelectric films," *Nat. Commun.* **8**, 15549 (2017).
- <sup>16</sup>M. Stengel, D. Vanderbilt, and N. A. Spaldin, "First-principles modeling of ferroelectric capacitors via constrained displacement field calculations," *Phys. Rev. B* **80**, 224110 (2009).
- <sup>17</sup>E. A. Eliseev, A. N. Morozovska, G. S. Svezhnikov, E. L. Rumyantsev, E. I. Shishkin, V. Y. Shur, and S. V. Kalinin, "Screening and retardation effects on 180°-domain wall motion in ferroelectrics: Wall velocity and nonlinear dynamics due to polarization-screening charge interactions," *Phys. Rev. B* **78**, 245409 (2008).
- <sup>18</sup>E. A. Eliseev, A. N. Morozovska, S. V. Kalinin, Y. Li, J. Shen, M. D. Glinchuk, L.-Q. Chen, and V. Gopalan, "Surface effect on domain wall width in ferroelectrics," *J. Appl. Phys.* **106**, 084102 (2009).
- <sup>19</sup>M. Stengel and N. A. Spaldin, "Origin of the dielectric dead layer in nanoscale capacitors," *Nature* **443**, 679 (2006).
- <sup>20</sup>Y. Wang, M. K. Niranjana, K. Janicka, J. P. Velev, M. Y. Zhuravlev, S. S. Jaswal, and E. Y. Tsymlar, "Ferroelectric dead layer driven by a polar interface," *Phys. Rev. B* **82**, 094114 (2010).
- <sup>21</sup>L. Pintilie and M. Alexe, "Metal-ferroelectric-metal heterostructures with Schottky contacts. I: Influence of the ferroelectric properties," *J. Appl. Phys.* **98**, 124103 (2005).
- <sup>22</sup>Y. Zhang, G.-P. Li, T. Shimada, J. Wang, and T. Kitamura, "Disappearance of ferroelectric critical thickness in epitaxial ultrathin BaZrO<sub>3</sub> films," *Phys. Rev. B* **90**, 184107 (2014).
- <sup>23</sup>V. Garcia, S. Fusil, K. Bouzehouane, S. Enouz-Vedrenne, N. D. Mathur, A. Barthélémy, and M. Bibes, "Giant tunnel electroresistance for non-destructive readout of ferroelectric states," *Nature* **460**, 81 (2009).
- <sup>24</sup>S. R. Lee, L. Baasandorj, J. W. Chang, I. W. Hwang, J. R. Kim, J.-G. Kim, K.-T. Ko, S. B. Shim, M. W. Choi, M. You, C.-H. Yang, J. Kim, and J. Song, "First observation of ferroelectricity in ~1 nm ultrathin semiconducting BaTiO<sub>3</sub> films," *Nano Lett.* **19**, 2243 (2019).
- <sup>25</sup>F. Liu, L. You, K. L. Seyler, X. Li, P. Yu, J. Lin, X. Wang, J. Zhou, H. Wang, H. He, S. T. Pantelides, W. Zhou, P. Sharma, X. Xu, P. M. Ajayan, J. Wang, and Z. Liu, "Room-temperature ferroelectricity in CuInP<sub>2</sub>S<sub>6</sub> ultrathin flakes," *Nat. Commun.* **7**, 12357 (2016).
- <sup>26</sup>W. Ding, J. Zhu, Z. Wang, Y. Gao, D. Xiao, Y. Gu, Z. Zhang, and W. Zhu, "Prediction of intrinsic two-dimensional ferroelectrics in In<sub>2</sub>Se<sub>3</sub> and other III<sub>2</sub>-VI<sub>3</sub> van der Waals materials," *Nat. Commun.* **8**, 14956 (2017).
- <sup>27</sup>S. Yuan, X. Luo, H. L. Chan, C. Xiao, Y. Dai, M. Xie, and J. Hao, "Room-temperature ferroelectricity in MoTe<sub>2</sub> down to the atomic monolayer limit," *Nat. Commun.* **10**, 1775 (2019).
- <sup>28</sup>J. A. Brehm, S. M. Neumayer, L. Tao, A. O'Hara, M. Chyasnachichus, M. A. Susner, M. A. McGuire, S. V. Kalinin, S. Jesse, P. Ganesh, S. T. Pantelides, P. Maksymovych, and N. Balke, "Tunable quadruple-well ferroelectric van der Waals crystals," *Nat. Mater.* **19**, 43 (2020).

- <sup>29</sup>V. Maisonneuve, V. B. Cajipe, A. Simon, R. Von Der Muhll, and J. Ravez, "Ferrielectric ordering in lamellar  $\text{CuInP}_2\text{S}_6$ ," *Phys. Rev. B* **56**, 10860 (1997).
- <sup>30</sup>L. You, Y. Zhang, S. Zhou, A. Chaturvedi, S. A. Morris, F. Liu, L. Chang, D. Ichinose, H. Funakubo, W. Hu, T. Wu, Z. Liu, S. Dong, and J. Wang, "Origin of giant negative piezoelectricity in a layered van der Waals ferroelectric," *Sci. Adv.* **5**, eaav3780 (2019).
- <sup>31</sup>S. M. Neumayer, L. Tao, A. O'Hara, J. Brehm, M. Si, P. Y. Liao, T. Feng, S. V. Kalinin, P. D. Ye, S. T. Pantelides, P. Maksymovych, and N. Balke, "Alignment of polarization against an electric field in van der Waals ferroelectrics," *Phys. Rev. Appl.* **13**, 064063 (2020).
- <sup>32</sup>S. M. Neumayer, L. Tao, A. O'Hara, M. A. Susner, M. A. McGuire, P. Maksymovych, S. T. Pantelides, and N. Balke, "The concept of negative capacitance in ionically conductive van der Waals ferroelectrics," *Adv. Energy Mater.* **10**, 2001726 (2020).
- <sup>33</sup>D. D. Xu, R. R. Ma, Y. F. Zhao, Z. Guan, Q. L. Zhong, R. Huang, P. H. Xiang, N. Zhong, and C. G. Duan, "Unconventional out-of-plane domain inversion via in-plane ionic migration in a van der Waals ferroelectric," *J. Mater. Chem. C* **8**, 6966 (2020).
- <sup>34</sup>J. Quereda, R. Biele, G. Rubio-Bollinger, N. Agraït, R. D'Agosta, and A. Castellanos-Gomez, "Strong quantum confinement effect in the optical properties of ultrathin  $\alpha\text{-In}_2\text{Se}_3$ ," *Adv. Opt. Mater.* **4**, 1939 (2016).
- <sup>35</sup>W. F. Io, S. Yuan, S. Y. Pang, L. W. Wong, J. Zhao, and J. Hao, "Temperature- and thickness-dependence of robust out-of-plane ferroelectricity in CVD grown ultrathin van der Waals  $\alpha\text{-In}_2\text{Se}_3$  layers," *Nano Res.* **13**, 1897 (2020).
- <sup>36</sup>Y. Li, C. Chen, W. Li, X. Mao, H. Liu, J. Xiang, A. Nie, Z. Liu, W. Zhu, and H. Zeng, "Orthogonal electric control of the out-of-plane field-effect in 2D ferroelectric  $\alpha\text{-In}_2\text{Se}_3$ ," *Adv. Electron. Mater.* **6**, 2000061 (2020).
- <sup>37</sup>S. N. Shirodkar and U. V. Waghmare, "Emergence of ferroelectricity at a metal-semiconductor transition in a 1T monolayer of  $\text{MoS}_2$ ," *Phys. Rev. Lett.* **112**, 157601 (2014).
- <sup>38</sup>C. Xiao, Z.-A. Xu, X. Luo, and Y. Lu, "Origin and electronic behavior of improper ferroelectricity in  $\text{AB}_2$  ( $\text{A} = \text{Cr, Mo, W}$ ;  $\text{B} = \text{S, Se, Te}$ ) transition metal dichalcogenides," *arXiv:2001.03164[cond-mat.mes-hall]* (2020).
- <sup>39</sup>W. Hou, A. Azizimanesh, A. Sewaket, T. Peña, C. Watson, M. Liu, H. Askari, and S. M. Wu, "Strain-Based room-temperature non-volatile  $\text{MoTe}_2$  ferroelectric phase change transistor," *Nat. Nanotechnol.* **14**, 668 (2019).
- <sup>40</sup>S. Singh, J. Kim, K. M. Rabe, and D. Vanderbilt, "Engineering weyl phases and nonlinear Hall effects in  $\text{Td-MoTe}_2$ ," *Phys. Rev. Lett.* **125**, 046402 (2020).
- <sup>41</sup>Y. Liu, N. O. Weiss, X. Duan, H.-C. Cheng, Y. Huang, and X. Duan, "Van der Waals heterostructures and devices," *Nat. Rev. Mater.* **1**, 16042 (2016).
- <sup>42</sup>Z.-Z. Sun, W. Xun, L. Jiang, J.-L. Zhong, and Y.-Z. Wu, "Strain engineering to facilitate the occurrence of 2D ferroelectricity in  $\text{CuInP}_2\text{S}_6$  monolayer," *J. Phys. D: Appl. Phys.* **52**, 465302 (2019).
- <sup>43</sup>J. R. Reimers, S. A. Tawfik, and M. J. Ford, "Van der Waals forces control ferroelectric-antiferroelectric ordering in  $\text{CuInP}_2\text{S}_6$  and  $\text{CuBiP}_2\text{Se}_6$  laminar materials," *Chem. Sci.* **9**, 7620 (2018).
- <sup>44</sup>A. Simon, J. Ravez, V. Maisonneuve, C. Payen, and V. B. Cajipe, "Paraelectric-ferroelectric transition in the lamellar thiophosphate  $\text{CuInP}_2\text{S}_6$ ," *Chem. Mater.* **6**, 1575 (1994).
- <sup>45</sup>S. A. Tawfik, J. R. Reimers, C. Stampfl, and M. J. Ford, "Van der Waals forces control the internal chemical structure of monolayers within the lamellar materials  $\text{CuInP}_2\text{S}_6$  and  $\text{CuBiP}_2\text{Se}_6$ ," *J. Phys. Chem. C* **122**, 22675 (2018).
- <sup>46</sup>M. Si, P.-Y. Liao, G. Qiu, Y. Duan, and P. D. Ye, "Ferroelectric field-effect transistors based on  $\text{MoS}_2$  and  $\text{CuInP}_2\text{S}_6$  two-dimensional van der Waals heterostructure," *ACS Nano* **12**, 6700 (2018).
- <sup>47</sup>X. Wang, P. Yu, Z. Lei, C. Zhu, X. Cao, F. Liu, L. You, Q. Zeng, Y. Deng, C. Zhu, J. Zhou, Q. Fu, J. Wang, Y. Huang, and Z. Liu, "Van der Waals negative capacitance transistors," *Nat. Commun.* **10**, 3037 (2019).
- <sup>48</sup>M. Zhao, G. Gou, X. Ding, and J. Sun, "An ultrathin two-dimensional vertical ferroelectric tunneling junction based on  $\text{CuInP}_2\text{S}_6$  monolayer," *Nanoscale* **12**, 12522 (2020).
- <sup>49</sup>X. Jin, Y. Zhang, S. T. Pantelides, and S. Du, "Integration of graphene and two-dimensional ferroelectrics: Properties and related functional devices," *Nanoscale Horiz.* **5**, 1303 (2020).
- <sup>50</sup>W. Huang, F. Wang, L. Yin, R. Cheng, Z. Wang, M. G. Sendeku, J. Wang, N. Li, Y. Yao, and J. He, "Gate-coupling-enabled robust hysteresis for nonvolatile memory and programmable rectifier in van der Waals ferroelectric heterojunctions," *Adv. Mater.* **32**, 1908040 (2020).
- <sup>51</sup>M. S. Choi, B. K. Cheong, C. H. Ra, S. Lee, J.-H. Bae, S. Lee, G.-D. Lee, C.-W. Yang, J. Hone, and W. J. Yoo, "Electrically driven reversible phase changes in layered  $\text{In}_2\text{Se}_3$  crystalline film," *Adv. Mater.* **29**, 1703568 (2017).
- <sup>52</sup>A. M. Kolpak, N. Sai, and A. M. Rappe, "Short-circuit boundary conditions in ferroelectric  $\text{PbTiO}_3$  thin films," *Phys. Rev. B* **74**, 054112 (2006).
- <sup>53</sup>G. Kresse and J. Furthmüller, "Efficient iterative schemes for *ab initio* total-energy calculations using a plane-wave basis set," *Phys. Rev. B* **54**, 11169 (1996).
- <sup>54</sup>G. Kresse and D. Joubert, "From ultrasoft pseudopotentials to the projector augmented-wave method," *Phys. Rev. B* **59**, 1758 (1999).
- <sup>55</sup>P. E. Blöchl, "Projector augmented-wave method," *Phys. Rev. B* **50**, 17953 (1994).
- <sup>56</sup>J. P. Perdew, K. Burke, and M. Ernzerhof, "Generalized gradient approximation made simple," *Phys. Rev. Lett.* **77**, 3865 (1996).
- <sup>57</sup>A. D. Becke and E. R. Johnson, "A density-functional model of the dispersion interaction," *J. Chem. Phys.* **123**, 154101 (2005).
- <sup>58</sup>S. Grimme, S. Ehrlich, and L. Goerigk, "Effect of the damping function in dispersion corrected density functional theory," *J. Comput. Chem.* **32**, 1456 (2011).
- <sup>59</sup>H. J. Monkhorst and J. D. Pack, "Special points for brillouin-zone integrations," *Phys. Rev. B* **13**, 5188 (1976).
- <sup>60</sup>G. Henkelman, B. P. Uberuaga, and H. Jonsson, "A climbing image nudged elastic band method for finding saddle points and minimum energy paths," *J. Chem. Phys.* **113**, 9901 (2000).
- <sup>61</sup>G. Henkelman and H. Jonsson, "Improved tangent estimate in the nudged elastic band method for finding minimum energy paths and saddle points," *J. Chem. Phys.* **113**, 9978 (2000).
- <sup>62</sup>B. Meyer and D. Vanderbilt, "*Ab initio* study of  $\text{BaTiO}_3$  and  $\text{PbTiO}_3$  surfaces in external electric fields," *Phys. Rev. B* **63**, 205426 (2001).
- <sup>63</sup>S. M. Neumayer, M. Si, J. Li, P.-Y. Liao, L. Tao, A. O'Hara, S. T. Pantelides, P. D. Ye, P. Maksymovych, and N. Balke, "Ionic control over ferroelectricity in 2D layered van der Waals capacitors," *ACS Appl. Mater. Interfaces* **14**, 3018 (2022).
- <sup>64</sup>A. A. Marakushev and N. I. Bezmen, "Chemical affinity of metals for oxygen and sulfur," *Int. Geol. Rev.* **13**, 1781 (1971).
- <sup>65</sup>S. M. Neumayer, J. A. Brehm, L. Tao, A. O'Hara, P. Ganesh, S. Jesse, M. A. Susner, M. A. McGuire, S. T. Pantelides, P. Maksymovych, and N. Balke, "Local strain and polarization mapping in ferrielectric materials," *ACS Appl. Mater. Interfaces* **12**, 38546 (2020).
- <sup>66</sup>S. M. Neumayer, Z. Zhao, A. O'Hara, M. A. McGuire, M. A. Susner, S. T. Pantelides, P. Maksymovych, and N. Balke, "Nanoscale control of polar surface phases in layered van der Waals  $\text{CuInP}_2\text{S}_6$ ," *ACS Nano* **16**, 2452 (2022).